ARTICLES

Mediators of vascular remodelling co-opted for sequential steps in lung metastasis

Gaorav P. Gupta[1]*, Don X. Nguyen[1]*, Anne C. Chiang[1,2], Paula D. Bos[1], Juliet Y. Kim[1], Cristina Nadal[1]†, Roger R. Gomis[1]†, Katia Manova-Todorova[3] & Joan Massagué[1,4]

Metastasis entails numerous biological functions that collectively enable cancerous cells from a primary site to disseminate and overtake distant organs. Using genetic and pharmacological approaches, we show that the epidermal growth factor receptor ligand epiregulin, the cyclooxygenase COX2, and the matrix metalloproteinases 1 and 2, when expressed in human breast cancer cells, collectively facilitate the assembly of new tumour blood vessels, the release of tumour cells into the circulation, and the breaching of lung capillaries by circulating tumour cells to seed pulmonary metastasis. These findings reveal how aggressive primary tumorigenic functions can be mechanistically coupled to greater lung metastatic potential, and how such biological activities may be therapeutically targeted with specific drug combinations.

The emergence of disseminated metastases remains the primary cause of mortality in cancer patients[1–3]. Recent searches for genetic determinants of metastasis have led to the identification of gene sets, or 'signatures', for which the expression in primary tumours is associated with high risk of metastasis and poor disease survival[4–10]. It has been proposed that the expression of such genes in primary tumours might directly predispose cancer cells for growth in distant organs[11], raising questions about the distinction between tumorigenic genes and genes that mediate metastasis. A contrasting, long-held view is that metastasis arises from rare tumour cell clones, the genetic make-up of which endows them with a unique selective advantage in distant organ microenvironments[1]. Breast cancer metastasis genes that may correspond to each of these two models have been recently identified in a functional screen for mediators of lung colonization[12]. A subset of the genes identified in this manner supports mammary tumour growth as well as pulmonary metastasis by human cancer cells in mice, and constitutes a lung metastasis gene signature (LMS), the expression of which in primary tumours indicates a high risk of pulmonary relapse in breast cancer patients[12,13]. Other genes emerging from the same screen, however, imparted lung metastasis virulence without affecting primary tumour growth[12]. The specific roles that these various genes may have in metastasis have remained unknown.

Here we report that four LMS genes collectively contribute vascular remodelling functions that can support the formation of vasculature in mammary tumours, the entry of tumour cells into the circulation and the exit of tumour cells from the bloodstream into the lung parenchyma. Their ability to mediate distinct functions in the primary site and in the lung metastasis setting distinguishes these genes from oncogenes that primarily support the transformed state in cancer cells. The present findings suggest a molecular basis for the lung metastasis proclivity of locally aggressive primary breast tumours, and a rationale for combinatorial therapeutic interventions against metastasis.

Genetic cooperation in mammary tumour growth

The MDA-MB-231 cell line, which was derived from the pleural fluid of a patient with widely metastatic breast cancer[14], is a heterogeneous population composed of cells with diverse organotropic metastatic potential and distinct pro-metastatic gene expression signatures[15–17]. Notably, some of the LMS genes that typify the lung metastatic subpopulations derived from this source were independently identified as downstream effectors of vascular endothelial growth factor (VEGF) in endothelial cells[18]. This suggested to us the possibility that, when expressed by tumour cells, these genes may confer vascular remodelling functions that are relevant for metastatic progression. These genes include the epidermal growth factor receptor (EGFR)/pan-HER ligand epiregulin (*EREG*), the prostaglandin-synthesizing enzyme cyclooxygenase 2 (*COX2*; also called *PTGS2*), and the matrix-remodelling metalloproteinases *MMP1* and *MMP2*. *EREG*, *COX2* and *MMP1* are part of the clinically validated LMS genes and *MMP2* is frequently associated with them[12]. Unlike endothelial cells[18], the lung metastatic MDA-MB-231 subpopulation LM2-4175 (hereafter called LM2) expressed these four genes in a manner that was neither dependent on autocrine VEGF (Supplementary Fig. 1a, b) nor responsive to VEGF addition (Supplementary Fig. 1c). Thus, we investigated whether the elevated expression of these genes in cancer cells might recapitulate a transcriptional programme encoding secretory mediators of vascular remodelling for tumorigenesis and lung metastasis.

We stably reduced the expression of *EREG*, *COX2*, *MMP1* and *MMP2* by using short hairpin RNA interference (shRNA) in LM2 cells[12]. We also generated compound knockdown cells in which up to four shRNAs were expressed in a given cell population, attaining significant silencing of all targeted genes and their encoded products (Fig. 1a and Supplementary Fig. 2). The extent of silencing achieved is consistent with multiple constructs being simultaneously active in most, but not all, cells in the knockdown population. Reduction of *EREG*, *COX2*, *MMP1* or *MMP2* expression individually had statistically significant, yet limited, effects on tumour growth on cell inoculation into the mammary fat pad of immunocompromised mice (Fig. 1b, left graph). Nevertheless, silencing of these genes in different combinations delayed tumour progression, with nearly complete abrogation of growth achieved by silencing all four genes simultaneously (Fig. 1b, right graph). Each cell line was infected with similar

[1]Cancer Biology and Genetics Program, [2]Department of Medicine, [3]Molecular Cytology Core Facility, and [4]Howard Hughes Medical Institute, Memorial Sloan-Kettering Cancer Center, New York, New York 10021, USA. †Present addresses: Hemato-Oncology Institute, Hospital Clinic de Barcelona, 08036 Barcelona, Spain (C.N.); Oncology Programme, Institute for Research in Biomedecine, Barcelona Science Park and University of Barcelona, 08028 Barcelona, Spain (R.R.G.).
*These authors contributed equally to this work.

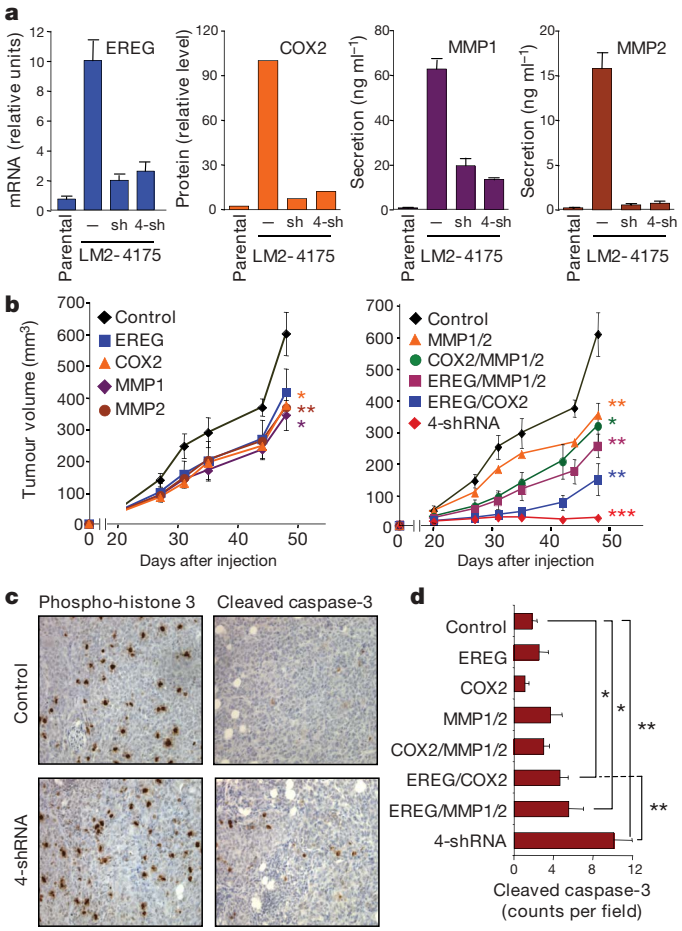

Figure 1 | *EREG*, *MMP1*, *MMP2* and *COX2* cooperate to mediate primary tumour growth. **a**, LM2 cells were infected with retrovirus encoding a control hairpin, or with shRNAs targeting *EREG*, *MMP1*, *MMP2* or *COX2*. For combination knockdown retrovirus, multiple hairpin vectors were transfected as pools into viral packaging cell lines. Infected cells were selected and *EREG* knockdown was determined by quantitative (q)RT–PCR, COX2 analysed via western blot, and secreted MMP1 and MMP2 measured by ELISA. Shown are levels of each gene product in the parental MDA-MB-231 cell line from which LM2 cells were selected, as well as LM2 control, single (sh) and quadruple knockdown (4-sh) cells. $n = 3$; error bars represent 95% confidence interval for qRT–PCR analysis and standard errors of the mean (s.e.m.) for ELISA. **b**, 1×10^6 cells of control, single knockdowns, or the indicated combination knockdown samples were inoculated into the fourth mammary fat pads of immunodeficient mice. Length and width of palpable tumours were measured, and tumour volumes calculated at the indicated time points. Left: effects of single gene knockdown; right: control compared to combination knockdown cells. $n = 6$; error bars indicate s.e.m.; asterisk, $P < 0.05$; double asterisk, $P < 0.01$; triple asterisk, $P < 0.001$; calculated using a two-tailed Student's *t*-test for tumour volumes at the last time point, compared to control. **c**, Automated immunohistochemistry for phospho-histone 3 and cleaved caspase-3 detection was performed on tumours obtained from the various combination knockdown cell lines. Shown are representative images at an original magnification of ×20. **d**, Quantification of cleaved caspase-3 staining using Image J software. $n = 15$; error bars indicate s.e.m.; single asterisk, $P < 0.01$; double asterisk, $P < 0.001$; calculated using a two-sided Wilcoxon rank-sum test, compared to levels in control tumours.

retroviral titres irrespective of the number of different hairpin sequences introduced. Moreover, overexpression of MMP1, MMP2 and COX2 in the context of cells targeted by all four shRNAs resulted in phenotypic rescue of tumour growth to levels that were observed for the single *EREG* knockdown (Supplementary Fig. 3a, b). The combined knockdown of three lung metastasis virulence genes, *IL13RA2*, *SPARC* and *VCAM1* (ref. 12), only mildly affected mammary tumour growth despite strongly inhibiting lung metastasis (Supplementary Fig. 3d–f). Thus, not all combinations of lung metastasis mediators stimulate primary tumorigenesis. Overall, these results uncover specific genetic interactions between *EREG*, *MMP1*, *MMP2* and *COX2* that collectively facilitate accelerated mammary tumour growth.

Quantified phosphorylated histone H3 levels indicated that none of the single or combined knockdowns of these genes significantly altered the proliferation rate of the tumour cells (Fig. 1c and Supplementary Fig. 4a). In contrast, an increased rate of apoptosis was evident in tumours with combinatorial knockdown, as measured by cleaved caspase-3 staining (Fig. 1c, d). Dual inhibition of *EREG* and *COX2* resulted in a synergistic rise in the rate of primary tumour apoptosis (Supplementary Fig. 4b). Although further inhibition of *MMP1* and *MMP2* did not reach the statistical threshold for synergy, reduction of these genes resulted in a supra-additive effect above the level of apoptosis observed in the *EREG*/*COX2* knockdown (Supplementary Fig. 4c).

Role in mammary tumour angiogenesis

Increased rates of tumour cell death might be secondary to defects in angiogenesis. Indeed, histological staining for endothelial cell marker CD31 revealed profound defects in the vascular morphology of tumours that had reduced expression of all four of these lung metastasis genes (Fig. 2a). Digital imaging analysis and quantification of vessel structure demonstrated that although the average number of discrete vessel units was not considerably altered, the length, number of lumens and extent of branching of the existing vasculature were significantly reduced in the combined knockdown tumours (Fig. 2b). These morphological changes were also visualized using CD31 immunofluorescence and confocal microscopy to image the tumour vasculature (Supplementary Fig. 5). Co-staining for CD31 and NG2, a smooth muscle pericyte marker, did not reveal any major differences in pericyte recruitment (Supplementary Fig. 5b). Nevertheless, vessels in the quadruple knockdown tumours exhibited diminished effusion of intravenously injected dextran, consistent with attenuated vascular permeability (Fig. 2c). Of note, these defects in primary tumour vessel morphology and function occurred in the absence of differences in VEGF levels between control and knockdown tumour cells (Supplementary Fig. 1a). This suggested that the aforementioned genes promote the formation of the dilated, tortuous and

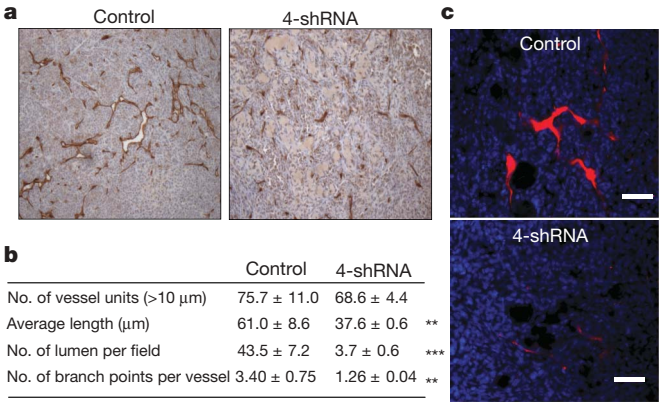

b

	Control	4-shRNA	
No. of vessel units (>10 μm)	75.7 ± 11.0	68.6 ± 4.4	
Average length (μm)	61.0 ± 8.6	37.6 ± 0.6	**
No. of lumen per field	43.5 ± 7.2	3.7 ± 0.6	***
No. of branch points per vessel	3.40 ± 0.75	1.26 ± 0.04	**

Figure 2 | *EREG*, *MMP1*, *MMP2* and *COX2* mediate tumour angiogenic progression. **a**, Automated anti-CD31 immunohistochemistry was performed on control and 4-shRNA-targeted tumours. Representative images were obtained at ×10 magnification. **b**, Tumour sections stained with anti-CD31 antibody were used for morphometric vessel analysis. Vessel units (defined as ≥10 μm in length), vessel length, number of lumen and average number of branch points were quantified as described in Methods. $n = 15$; error bars indicate s.e.m.; double asterisk, $P < 0.01$; triple asterisk, $P < 0.001$; calculated using a two-tailed Student's *t*-test. **c**, Mice bearing tumours were injected with rhodamine-conjugated dextran. Tumours were extracted and sections examined for vessel permeability at ×10 magnification. Scale bars, 50 μm.

leaky blood vessels that typify the neovasculature of aggressive primary tumours[19].

Tumour cell extravasation from lung capillaries

To assess the importance of these genes as mediators of pulmonary colonization, the knockdown lines were injected intravenously into mice, and lung metastatic progression was monitored by bioluminescence (Fig. 3a) and histological examination (Supplementary Fig. 6a). Independent silencing of these genes had little impact in this lung colonization assay. As in the mammary tumorigenesis assays, inhibition of lung colonization was attained when these genes were silenced in combination, with knockdown of all four genes yielding the most salient defect. Metastatic colonies were eventually observed in the combination knockdown samples, but this was attributable to outgrowth of cells escaping knockdown and re-expressing these genes (data not shown). Statistical tests identified multiple synergistic interactions between *EREG*, *COX2*, *MMP1* and *MMP2* in the early progression of lung metastasis (Supplementary Fig. 6b). The specificity of this phenotype was confirmed by overexpressing MMP1, MMP2 and COX2, which resulted in significant recovery of lung metastatic activity (Supplementary Fig. 3c).

To visualize lung metastasis events during the initial days after inoculation, whole lungs were extracted and scanned by confocal microscopy. Within 2 days of entering the circulation, control tumour cells could be visualized outside of the lung capillaries, showing that they efficiently extravasate into the lung parenchyma (Fig. 3b, left panel). Conversely, when detected, the knockdown cells in which all four genes were targeted by shRNAs were trapped within vessels as single cells, seemingly incapable of breaching the lung endothelium (Fig. 3b, right panel). In an *in vitro* assay of trans-endothelial migration, the migratory capacity of LM2 cells through an endothelial monolayer was inhibited by the combined knockdown of all four genes, which did not entail a generalized defect in cell motility (Fig. 3c and Supplementary Fig. 7). Thus, although several mechanisms and outcomes have been proposed for interactions between EGFR/HER, MMPs and COX2[20–23], our results provide evidence that the expression of EREG, COX2, MMP1 and MMP2 by cancer cells can collectively promote metastatic extravasation in the lungs.

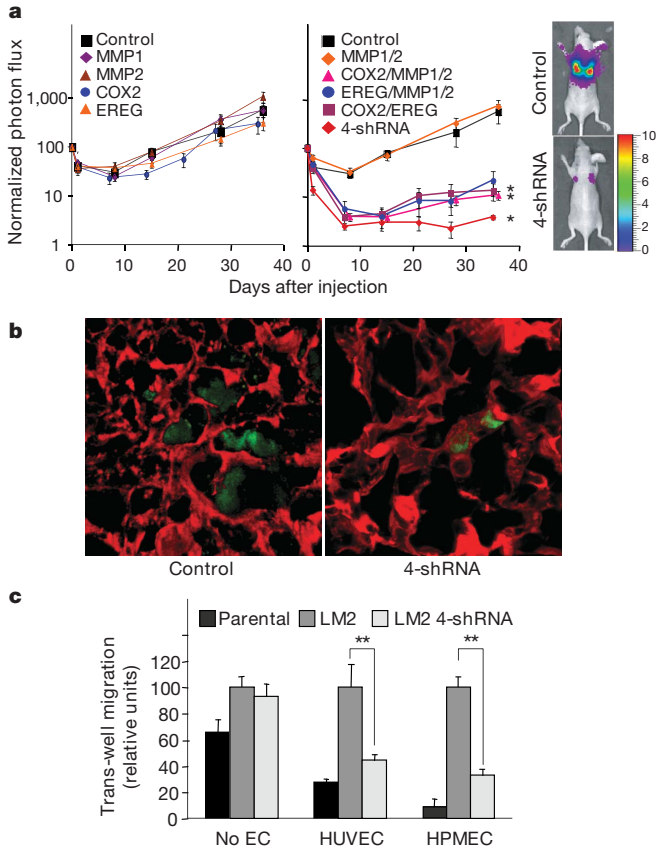

Figure 3 | Genetic inhibition of *EREG*, *MMP1*, *MMP2* and *COX2* prevents metastatic extravasation. a, Single and combination knockdown cells were inoculated intravenously into mice. Lung metastasis was measured by bioluminescence and quantified. Left: effects of single knockdowns versus control; right: effects of combination knockdowns versus control with representative bioluminescent images of mice injected with control and 4-shRNA-treated cells at day 35. $n = 5$; error bars indicate s.e.m.; asterisk, $P < 0.05$; based on a two-sided rank-sum test compared to shRNA control LM2 cells. **b**, Control or 4-shRNA-targeted cells were pulsed with cell tracker green and injected into the tail vein of mice. Forty-eight hours after tumour cell inoculation, animals were injected intravenously with rhodamine-conjugated lectin. Whole lungs were then extracted after necropsy and imaged by two-photon confocal microscopy at ×63 magnification. Three-dimensional reconstructed images of tumour cells (green) relative to lung capillaries (red) are shown. **c**, Indicated cell lines were seeded into trans-well inserts with or without (No EC) an endothelial monolayer. Images of cells migrating were captured at ×10 magnification and quantified with ImageJ software. Trans-endothelial migration was performed with either human umbilical vein endothelial cell (HUVEC) or human pulmonary microvascular endothelial cell (HPMEC) monolayers with similar results. $n = 6–10$; error bars indicate s.e.m.; double asterisk, $P < 0.01$; based on a two-sided Student's *t*-test.

Combined drug inhibition of tumour growth and dissemination

These metastasis-promoting activities can also be pharmacologically targeted using previously characterized doses of the anti-EGFR antibody cetuximab[24], the broad-spectrum MMP inhibitor GM6001[25] and the COX2 inhibitor celecoxib[26]. We used an orthotopic model to assess the efficacy of these drug combinations as interventions during the natural formation of lung metastasis from mammary tumours (Fig. 4a). When used as single agents, these drugs minimally inhibited tumour growth of LM2 cells in the mammary glands. However, consistent with our genetic studies, treatment with the cetuximab/celecoxib and cetuximab/celecoxib/GM6001 combinations reduced the rate of primary tumour growth (Fig. 4b). This was accompanied by vascular defects that precipitated tissue hypoxia and ensuing tumour cell apoptosis (Supplementary Fig. 8). This vascular phenotype is also consistent with the ability of cetuximab and celecoxib to inhibit angiogenesis by means of both autocrine and paracrine mechanisms[27,28].

We examined whether the vascular defects elicited by these drugs also resulted in impaired tumour cell intravasation from the primary site. To this end, the presence of circulating tumour cells was assessed by measuring the relative expression of human-specific *GAPDH* in blood from treated mice. Notably, both drug combinations (cetuximab/celecoxib and cetuximab/celecoxib/GM6001) diminished the presence of circulating tumour cells, with the effect of the cetuximab/celecoxib combination reaching statistical significance (Fig. 4c).

Despite the inhibitory effects on intravasation, we noticed that some tumour cells had already colonized the lungs of animals before the initiation of pharmacological treatment (day 24), as seen by immunofluorescent staining (data not shown). Moreover, a significant number of tumour cells were still detectable in the lungs of treated mice (Fig. 4d). Confocal imaging after staining for vascular endothelium and cancer cells showed that vehicle-treated mice harboured large lung metastatic lesions that had efficiently extravasated, whereas mice treated with the cetuximab/celecoxib and cetuximab/celecoxib/GM6001 combinations exhibited a strong bias towards smaller micrometastases that remained trapped within the lung vasculature (Fig. 4e). Digital image quantification of multiple lung sections established statistically significant inhibitory effects for both drug combinations on the overall lung metastatic burden, as well as on the size distribution of the lung metastasis lesions (Fig. 4f, g). GM6001 addition did not increase the inhibitory effects of the cetuximab/celecoxib combination.

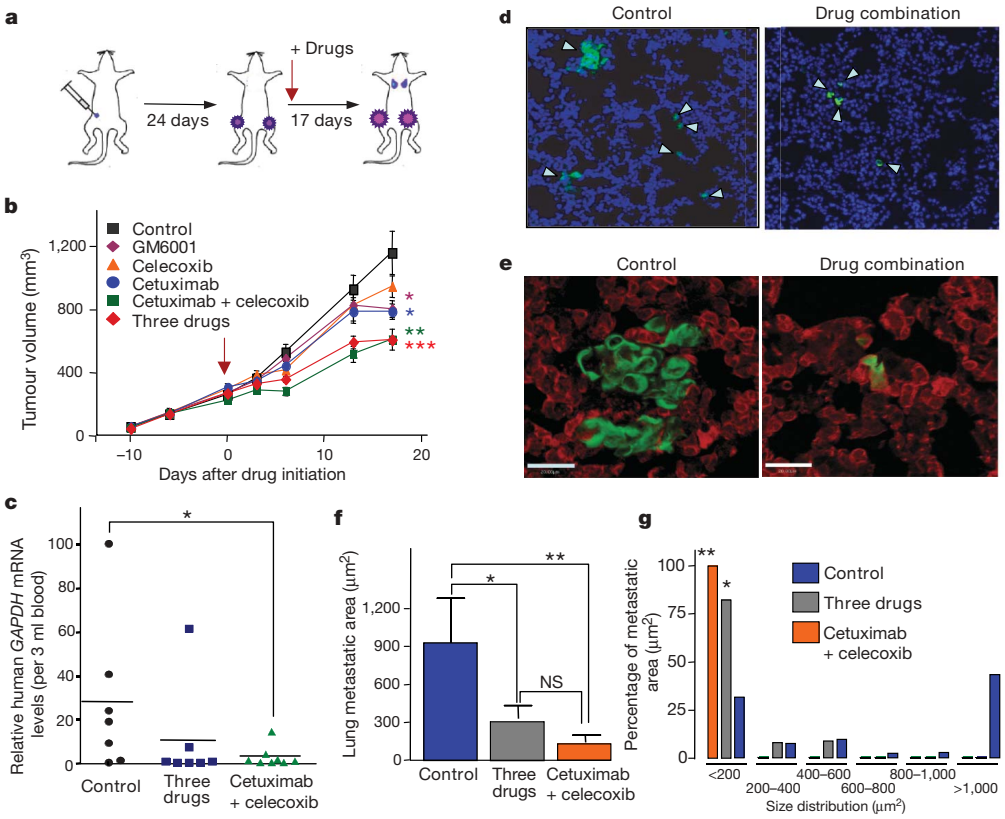

Figure 4 | Pharmacological inhibition of tumour growth and dissemination in orthotopically implanted primary tumours. **a**, Schematic representation of the time course for tumour cell implantation, primary tumour growth and therapeutic treatment to assess effects on primary tumour and lung metastatic progression. Animals were treated with vehicle control, cetuximab, celecoxib, GM6001, or the indicated combinations. **b**, Tumour volume measurements of mice treated with vehicle control or targeted therapies, either individually or in combination. $n = 6$; error bars indicate s.e.m.; asterisk, $P < 0.05$; double asterisk, $P < 0.01$; triple asterisk, $P < 0.001$; based on a two-sided Student's *t*-test, compared to control-treated animals. **c**, Blood from mice was isolated and red blood cells lysed. RNA from the remaining cells was extracted for qRT–PCR. The presence of circulating tumour cells was assessed as a function of human-specific *GAPDH* expression relative to murine *B2m*, in 3 ml of mouse blood perfusate. $n = 7$–8; bars indicate median *GAPDH* expression; asterisk, $P < 0.05$; based on a two-sided Student's *t*-test. **d**, Staining for tumour cells in lung cryosections using a human-specific vimentin antibody. Nuclei were visualized using 4,6-diamidino-2-phenylindole (DAPI). Arrowheads indicate tumour cell clusters in representative ×10 images of lungs from control (left) and animals treated with all three drugs (right). **e**, Confocal imaging at ×63 magnification of tumour cells (vimentin, green) and lung vasculature (lectin, red) from control (left) and treated animals (three drugs, right). Scale bars, 20 μm. **f**, Digital quantification of lung metastatic burden. Fluorescein isothiocyanate (FITC)-stained cancer cells in the lungs were quantified as metastatic lesions, and normalized to the area of nuclear DAPI staining. Shown on the graph is the average lung metastatic area per 5×10^5 μm^2 DAPI area. $n = 10$; error bars indicate s.e.m. **g**, Percentage of the lung metastatic burden that was occupied by lesions of the indicated sizes. **f**, **g**, Asterisk, $P < 0.05$; double asterisk, $P < 0.01$; NS, not significant, based on a two-tailed Wilcoxon rank-sum test.

Inhibiting lung colonization by metastatic cells

When used as single agents, these drugs also minimally inhibited pulmonary outgrowth of LM2 cells directly inoculated into the tail vein, whereas in combination these drugs prevented metastasis in a manner that mimicked the effects of genetic knockdown (Fig. 5a and Supplementary Fig. 9a). An exception to this trend was the antagonistic interaction between celecoxib and GM6001, perhaps reflecting the fact that the latter is a broad-spectrum MMP inhibitor, likely to affect both pro- and anti-metastatic MMPs[29]. Although the interactions between these agents did not achieve statistical thresholds for synergy, the combination of cetuximab and celecoxib, as well as of cetuximab and GM6001, resulted in supra-additive inhibition of lung metastasis (Supplementary Fig. 9b). Consistent with the genetic inhibition studies, combined pharmacological intervention resulted in the capillary entrapment of the remaining tumour cells even when visualized 4 weeks after tumour cell inoculation (Fig. 5b). Interestingly, the inhibition of extravasation was reversed on discontinuation of drug treatment, with most of the remaining lesions expanding into colonies that invaded the lung parenchyma (Fig. 5b, right panel).

We performed similar experiments with malignant cells freshly obtained from the pleural fluid of two patients with advanced breast cancer and a diagnosis of lung metastasis who were undergoing routine therapeutic procedures at our institution. Carcinoma cells were isolated from these samples based on the epithelial cell marker EpCAM, under institutionally approved protocols[30]. One sample (CN34) was subjected to *in vivo* selection for metastasis-forming cells[12]. As with the MDA-MB-231 cell line, this process yielded a subpopulation (CN34.2A) that expresses high levels of *EREG*, *COX2* and *MMP1* compared with the unsorted CN34 population (Fig. 5c). This was associated with an elevated lung colonizing activity of CN34.2A cells in mice, which could be inhibited by the administration of cetuximab and celecoxib (Fig. 5d, e). A sample from a different patient (CN41) was used without prior experimental selection for metastatic cells. CN41 cells expressed higher levels of *EREG* and *COX2* than did MDA-MB-231 cells (Fig. 5c), and had basal lung colonizing activity that could also be inhibited by the celecoxib/cetuximab combination (Fig. 5d). In all cases the metastasis inhibitory effects of this combination were observed from the earliest stages of metastatic colonization (day 2) and were sustained over 5 weeks (data not shown). These results support the general relevance of these genes in lung colonization, and the ability to interfere with this process by combining their pharmacological inhibitors.

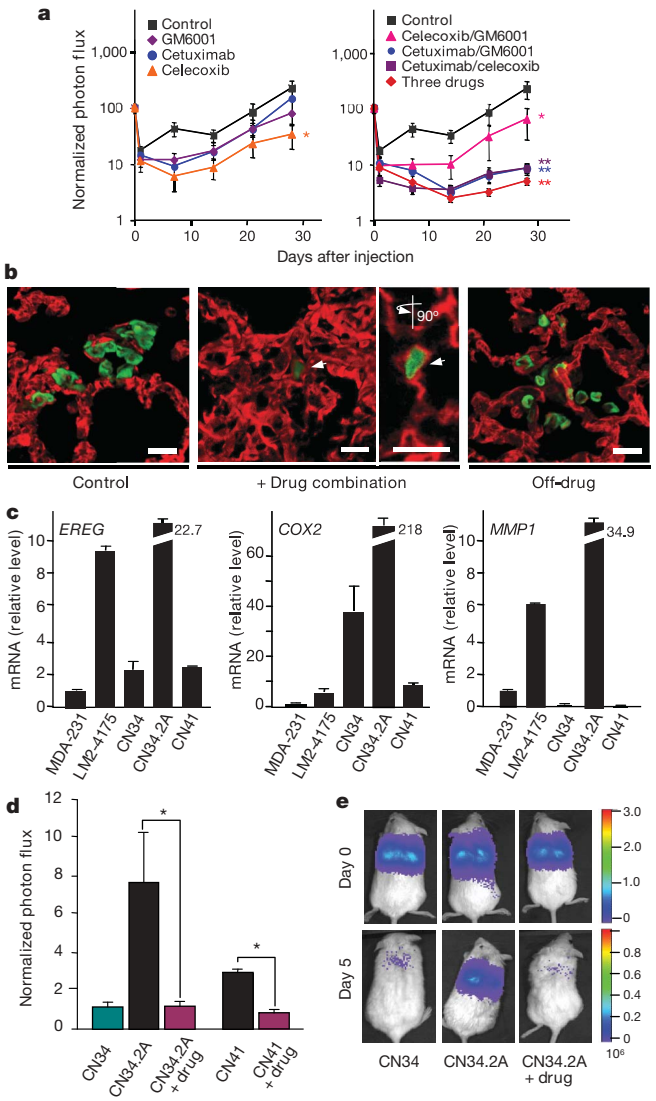

Figure 5 | Targeted inhibition of metastatic extravasation and lung colonization by LM2 and primary malignant cells. a, Mice were pre-treated with the indicated agents, 2 days before tumour cell inoculation. After intravenous injections of LM2 cells, drug treatment was maintained and lung metastasis quantified as in Fig. 2. Left: effects of single agents versus control; right: combination drug treatments versus control. $n = 5$; error bars indicate s.e.m.; asterisk, $P < 0.05$; double asterisk, $P < 0.01$; triple asterisk, $P < 0.001$; calculated using a two-sided rank-sum test compared to control treated animals. **b**, Lungs from control or cetuximab/celecoxib/GM6001 (drug combination)-treated mice were collected at day 28. Treatment was terminated in a subset of animals and mice were monitored for an additional 6 weeks. Lungs from these 'off-drug' mice were then collected after necropsy. Lung sections from vehicle-treated, drug-combination-treated and off-drug mice were processed for immunofluorescent detection of tumour-specific vimentin (green) and CD31 (red). Scale bars, 20 μm. **c**, Primary breast carcinoma cell populations CN34 and CN41 were isolated from the pleural effusion of patients. The CN34 derivative, CN34.2A, was obtained by *in vivo* selection of highly metastatic cells in mice. Expression of *EREG*, *COX2* and *MMP1* was assessed by qRT–PCR and compared to parental MDA-MB-231 and LM2 cell lines. $n = 3$; error bars represent 95% confidence interval. **d**, CN34, CN34.2A and CN41 were injected intravenously, mice were treated with cetuximab and celecoxib, and lung colonization was measured via bioluminescence. $n = 5$; error bars indicate s.e.m.; asterisk, $P < 0.05$; based on a two-sided rank-sum test. **e**, Representative luminescence images.

Discussion

Our current findings identify *EREG*, *COX2*, *MMP1* and *MMP2* as a subset of LMS genes that are co-opted by breast cancer cells and reconstitute a multi-functional vascular remodelling programme that promotes metastatic progression. In orthotopic primary tumour assays, these factors collectively mediate pathological angiogenic progression, with an ensuing increase in vascular permeability and tumour cell intravasation. Remarkably, this set of genes is also required to breach the lung vasculature and enable extravasation of cancer cells on dissemination of these cells from mammary tumours to the lungs. Although the individual targeting of these mediators was insufficient to prevent such biological activities, their combined inhibition resulted in profound reductions in sequential steps of metastatic progression.

The engagement of a common set of factors in distinct steps of metastasis qualifies them as 'metastasis progression' genes, which we define as genes that fulfil certain rate-limiting functions in primary tumour growth and other specific functions in metastatic colonization. Metastasis progression genes are thus distinguished from oncogenes that fulfil cell-autonomous transforming functions through the course of malignant disease, and from 'metastasis virulence' genes, defined as those genes that participate in metastatic colonization but not in primary tumour development.

Despite the major clinical advances provided by cytotoxic, hormonal and targeted therapies, the median survival after diagnosis of metastatic breast cancer with visceral organ involvement remains less than 2 years[31–33]. For the most part, the target of commonly used chemotherapy drugs continues to be the proliferation of cancer cells. As the molecular understanding of the biological functions necessary for metastasis increases, it may become possible to develop anti-metastatic strategies that target not only the intrinsic growth of disseminated tumour cells, but also their necessary interactions with newly adopted microenvironments. Our current observations demonstrate that inhibition of EGFR and COX2 can abate lung metastatic progression in a clinically relevant model of breast cancer. Collectively, these results identify extravasation as an essential step in metastatic progression that can be inhibited by combinatorial therapies formulated on the basis of biological insights.

METHODS SUMMARY

MDA-MB-231 and its lung metastatic derivative LM2-4175 have been described previously[12,17]. CN34 and CN41 carcinoma cells were isolated from the pleural effusion of patients with metastatic breast cancer treated at our institution on obtained written consent in accordance with IRB regulations, as previously described[30]. Metastatic cell subpopulations were obtained by *in vivo* selection in mice[12]. Knockdown of *MMP1*, *MMP2* and *COX2* was achieved using pRetroSuper technology[12]. For *EREG* targeting, an alternative vector was used (pSM2 derivative), which expresses the short hairpin embedded in a larger microRNA sequence[34]. All animal work was done in accordance with the MSKCC Institutional Animal Care and Use Committee. BALB/c nude and NOD/SCID female mice (NCI) age-matched between 5–7 weeks were used for xenografting studies. For inhibitor studies, 1 mg cetuximab was injected intraperitoneally bi-weekly, which yields plasma drug concentrations within the corresponding range in cetuximab-treated cancer patients[35]. GM6001 (Ryss Lab) was injected intraperitoneally at a dose of 2 mg kg^{-1} daily, which is efficacious in preclinical mouse models[25]. Celecoxib (LKT laboratories) was mixed with a powdered rodent chow diet (Research Diets) at a concentration of 1,000 parts per million, and provided continuously during the course of the experiment. Celecoxib serum concentrations in mice treated within this range are clinically attainable and sufficient to inhibit inflammation and prostaglandin synthesis in humans[22,26,36]. The Methods section provides additional information including cell culture, malignant cell isolation from pleural fluids, generation of retroviral gene-knockdown vectors, infections and transfections, analysis of RNA and protein expression, trans-endothelial migration assays, animal inoculation and bioluminescence imaging, sources and use of pharmacological inhibitors, *in vivo* intravasation assays, tumour histological and immunohistochemical analyses, vascular permeability assays, extravasation visualization, and image quantification.

Full Methods and any associated references are available in the online version of the paper at www.nature.com/nature.

Received 19 December 2006; accepted 21 March 2007.

1. Fidler, I. J. The pathogenesis of cancer metastasis: the 'seed and soil' hypothesis revisited. *Nature Rev. Cancer* **3**, 453–458 (2003).

2. Hynes, R. O. Metastatic potential: generic predisposition of the primary tumor or rare, metastatic variants—or both? *Cell* **113,** 821–823 (2003).
3. Gupta, G. P. & Massagué, J. Cancer metastasis: building a framework. *Cell* **127,** 679–695 (2006).
4. Perou, C. M. *et al.* Molecular portraits of human breast tumours. *Nature* **406,** 747–752 (2000).
5. van de Vijver, M. J. *et al.* A gene-expression signature as a predictor of survival in breast cancer. *N. Engl. J. Med.* **347,** 1999–2009 (2002).
6. Chang, H. Y. *et al.* Gene expression signature of fibroblast serum response predicts human cancer progression: similarities between tumors and wounds. *PLoS Biol.* **2,** E7 (2004).
7. Paik, S. *et al.* A multigene assay to predict recurrence of tamoxifen-treated, node-negative breast cancer. *N. Engl. J. Med.* **351,** 2817–2826 (2004).
8. Wang, Y. *et al.* Gene-expression profiles to predict distant metastasis of lymph-node-negative primary breast cancer. *Lancet* **365,** 671–679 (2005).
9. Bild, A. H. *et al.* Oncogenic pathway signatures in human cancers as a guide to targeted therapies. *Nature* **439,** 353–357 (2006).
10. Massagué, J. Sorting out breast-cancer gene signatures. *N. Engl. J. Med.* **356,** 294–297 (2007).
11. Bernards, R. & Weinberg, R. A. A progression puzzle. *Nature* **418,** 823 (2002).
12. Minn, A. J. *et al.* Genes that mediate breast cancer metastasis to lung. *Nature* **436,** 518–524 (2005).
13. Minn, A. J. *et al.* Lung metastasis genes couple breast tumor size and metastatic spread. *Proc. Natl Acad. Sci. USA* **104,** 6740–6745 (2007).
14. Cailleau, R., Young, R., Olive, M. & Reeves, W. J. Jr. Breast tumor cell lines from pleural effusions. *J. Natl Cancer Inst.* **53,** 661–674 (1974).
15. Gupta, G. P. *et al.* Identifying site-specific metastasis genes and functions. *Cold Spring Harb. Symp. Quant. Biol.* **70,** 1–10 (2005).
16. Kang, Y. *et al.* A multigenic program mediating breast cancer metastasis to bone. *Cancer Cell* **3,** 537–549 (2003).
17. Minn, A. J. *et al.* Distinct organ-specific metastatic potential of individual breast cancer cells and primary tumors. *J. Clin. Invest.* **115,** 44–55 (2005).
18. Wary, K. K., Thakker, G. D., Humtsoe, J. O. & Yang, J. Analysis of VEGF-responsive genes involved in the activation of endothelial cells. *Mol. Cancer* **2,** 25 (2003).
19. Carmeliet, P. & Jain, R. K. Angiogenesis in cancer and other diseases. *Nature* **407,** 249–257 (2000).
20. Krysan, K. *et al.* Prostaglandin E2 activates mitogen-activated protein kinase/Erk pathway signaling and cell proliferation in non-small cell lung cancer cells in an epidermal growth factor receptor-independent manner. *Cancer Res.* **65,** 6275–6281 (2005).
21. Dannenberg, A. J., Lippman, S. M., Mann, J. R., Subbaramaiah, K. & DuBois, R. N. Cyclooxygenase-2 and epidermal growth factor receptor: pharmacologic targets for chemoprevention. *J. Clin. Oncol.* **23,** 254–266 (2005).
22. Howe, L. R. *et al.* HER2/neu-induced mammary tumorigenesis and angiogenesis are reduced in cyclooxygenase-2 knockout mice. *Cancer Res.* **65,** 10113–10119 (2005).
23. Pai, R. *et al.* Prostaglandin E2 transactivates EGF receptor: a novel mechanism for promoting colon cancer growth and gastrointestinal hypertrophy. *Nature Med.* **8,** 289–293 (2002).
24. Goldstein, N. I., Prewett, M., Zuklys, K., Rockwell, P. & Mendelsohn, J. Biological efficacy of a chimeric antibody to the epidermal growth factor receptor in a human tumor xenograft model. *Clin. Cancer Res.* **1,** 1311–1318 (1995).
25. Gijbels, K., Galardy, R. E. & Steinman, L. Reversal of experimental autoimmune encephalomyelitis with a hydroxamate inhibitor of matrix metalloproteases. *J. Clin. Invest.* **94,** 2177–2182 (1994).
26. Jacoby, R. F., Seibert, K., Cole, C. E., Kelloff, G. & Lubet, R. A. The cyclooxygenase-2 inhibitor celecoxib is a potent preventive and therapeutic agent in the min mouse model of adenomatous polyposis. *Cancer Res.* **60,** 5040–5044 (2000).
27. Gately, S. & Li, W. W. Multiple roles of COX-2 in tumor angiogenesis: a target for antiangiogenic therapy. *Semin. Oncol.* **31,** 2–11 (2004).
28. Karashima, T. *et al.* Inhibition of angiogenesis by the antiepidermal growth factor receptor antibody ImClone C225 in androgen-independent prostate cancer growing orthotopically in nude mice. *Clin. Cancer Res.* **8,** 1253–1264 (2002).
29. Overall, C. M. & Kleifeld, O. Tumour microenvironment—opinion: validating matrix metalloproteinases as drug targets and anti-targets for cancer therapy. *Nature Rev. Cancer* **6,** 227–239 (2006).
30. Gomis, R. R., Alarcon, C., Nadal, C., Van Poznak, C. & Massagué, J. C/EBPβ at the core of the TGFβ cytostatic response and its evasion in metastatic breast cancer cells. *Cancer Cell* **10,** 203–214 (2006).
31. Giordano, S. H. *et al.* Is breast cancer survival improving? *Cancer* **100,** 44–52 (2004).
32. Solomayer, E. F., Diel, I. J., Meyberg, G. C., Gollan, C. & Bastert, G. Metastatic breast cancer: clinical course, prognosis and therapy related to the first site of metastasis. *Breast Cancer Res. Treat.* **59,** 271–278 (2000).
33. Baselga, J. & Norton, L. Focus on breast cancer. *Cancer Cell* **1,** 319–322 (2002).
34. Silva, J. M. *et al.* Second-generation shRNA libraries covering the mouse and human genomes. *Nature Genet.* **37,** 1281–1288 (2005).
35. Luo, F. R. *et al.* Correlation of pharmacokinetics with the antitumor activity of Cetuximab in nude mice bearing the GEO human colon carcinoma xenograft. *Cancer Chemother. Pharmacol.* **56,** 455–464 (2005).
36. Niederberger, E. *et al.* Celecoxib loses its anti-inflammatory efficacy at high doses through activation of NF-κB. *FASEB J.* **15,** 1622–1624 (2001).

Supplementary Information is linked to the online version of the paper at www.nature.com/nature.

Acknowledgements We thank A. Minn, D. Padua, C. Van Poznak, L. Norton, C. Hudis, Y. Pylayeva, P. Gupta, T. Westbrook and Z. Lazar for insightful discussions and technical suggestions. We also thank S. Tulley and members of the Molecular Cytology Core Facility for expert technical assistance. J.M. was funded by a National Institutes of Health grant, and by grants of the W. M. Keck Foundation and the Kleberg Foundation. G.P.G. is supported by an NIH Medical Scientist Training Program grant and a Department of Defense Breast Cancer Research Program pre-doctoral award. D.X.N. is a Berlex postdoctoral fellow of the Damon Runyon Cancer Research Foundation. A.C.C. was supported by an ASCO Young Investigator Award and by the Charles A. Dana Foundation. J.M. is an Investigator of the Howard Hughes Medical Institute.

Author Contributions J.M. designed and supervised experiments. G.P.G., D.X.N. and A.C.C. designed experiments; G.P.G., D.X.N., A.C.C., P.D.B. and J.Y.K. performed experiments; C.N. and R.R.G. isolated metastatic cells from clinical samples; K.T.-M. supervised histological and confocal microscopy imaging; J.M., G.P.G., D.X.N. and A.C.C. analysed data and wrote the manuscript. All authors discussed the results and commented on the manuscript.

Author Information Reprints and permissions information is available at www.nature.com/reprints. The authors declare no competing financial interests. Correspondence and requests for materials should be addressed to J.M. (j-massague@ski.mskcc.org).

METHODS

Cell culture. MDA-MB-231 and its lung metastatic derivative LM2-4175 have been described previously[12,17]. All tumour cell lines were cultured in DMEM supplemented with 10% FBS, glutamine, penicillin, streptomycin and fungizone. CN34 and CN41 carcinoma cells were isolated from the pleural effusion of patients with metastatic breast cancer treated at our institution upon written consent obtained following IRB regulations as previously described[30]. Briefly, pleural effusion samples were centrifuged at 1,000 r.p.m. for 10 min, cell pellets were re-suspended in PBS and treated with ACK lysis buffer to lyse blood cells. A fraction of these cells underwent negative selection to remove leukocytes ($CD45^+$ and $CD15^+$ cells), and EpCam-positive cells were sorted from the population upon recovery in tissue culture for 24 h. HUVEC (ScienCell) endothelial cells were cultured in complete ECM media (ScienCell), whereas primary human pulmonary microvascular endothelial cells (HPMECs, Cambrex) were cultured in EGM-2 (Cambrex). HUVECs and HPMECs were used between passages 3–6. The retroviral packaging cell line GPG29 was maintained in DMEM containing 10% FBS supplemented with puromycin, G418, doxycycline, penicillin, streptomycin and fungizone. Transfections were done using standard protocols with Lipofectamine 2000 (Invitrogen). After transfection, GPG29 cells were cultured in DMEM containing 10% FBS and sodium pyruvate.

Generation of retrovirus and knockdown cells. Knockdown of *MMP1*, *MMP2* and *COX2* was achieved using pRetroSuper technology targeting the following 19-nucleotide sequences: 5′-AGCGGAGAAATAGTGGCCC-3′ (*MMP1*), 5′-GGACGGACTCCTGGCTCAT-3′ (*MMP2*) and 5′-GGGCTGTCCCTTTACTT-CA-3′ (*COX2*). Knockdown of *IL13RA2*, *SPARC* and *VCAM1* was achieved as previously described[12]. For *EREG* targeting, an alternative vector was used (pSM2 derivative), which expresses the short hairpin embedded in a larger microRNA sequence[34]. The two target sequences used in the *EREG* gene were 5′-CCCAATATATTCTGACCGTTAA-3′ and 5′-ACCACAAATGCATAAAT-GCATA-3′. To produce retrovirus for combination knockdown, multiple hairpin vectors were transfected as pools into the GPG29 amphotropic packaging cell line. Viruses were collected 48 and 72 h after transfection, filtered, and concentrated by ultracentrifugation. Concentrated retrovirus was used to infect cells in the presence of 8 $\mu g\,ml^{-1}$ polybrene, typically resulting in a transduction rate of over 80%, and infected cells were selected with puromycin. Because the total amount of plasmid DNA used for co-transfection of multiple hairpins was the same as that used for single hairpin transfection, the combination knockdown retroviral titres were similar to titres attained when generating single knockdown virus. Moreover, we have demonstrated that up to four different vectors can be delivered and expressed efficiently in MDA-MB-231 cells using this protocol. Thus, knockdown cells obtained after drug selection were injected as a pooled population without subcloning. To generate knockdown-rescue cell lines, we used a similar method to produce virus encoding complementary DNAs for overexpression of the RNAi-targeted genes, along with a hygromycin selectable marker. Combination overexpressing retrovirus was used to super-infect previously generated knockdown cells that were subsequently selected with hygromycin.

Analysis of mRNA and protein expression. Total RNA from subconfluent MDA-MB-231 cells was collected and purified using the RNeasy kit (Qiagen). Five-hundred nanograms of total purified RNA was subjected to a reverse transcriptase reaction according to the SuperScript III first-strand synthesis system (Invitrogen). cDNA corresponding to approximately 5 ng of starting RNA was used for each of four replicates for quantitative PCR. Human *EREG*, *MMP1*, *MMP2*, *COX2* and *β2-microglobulin* (as an endogenous control) were amplified with commercially designed Taqman gene expression assays (Applied Biosystems) and the Taqman universal PCR master mix (Applied Biosystems). Quantitative expression data were acquired and analysed using an ABI Prism 7900HT Sequence Detection System (Applied Biosystems). For immunoblotting, cells were washed with PBS and lysed in RIPA buffer (50 mM Tris-HCl, pH 7.4, 1% NP-40, 0.25% Na-deoxycholate, 150 mM NaCl, 1 mM EDTA) supplemented with 50 mM NaF, 20 mM β-glycerophosphate, and complete protease inhibitor cocktail (Roche). Proteins were separated by SDS–PAGE and transferred to nitrocellulose membranes (Bio-Rad) that were immunoblotted with mouse monoclonal antibodies that recognize COX2 (Cayman Chemicals) and α-tubulin (Sigma). To facilitate detection of endogenous COX2 protein, cells were also pre-treated with 20 $ng\,ml^{-1}$ TNF-α for 5 h before lysing (R&D Systems). For analysis of secreted protein expression, cells were plated in triplicate at 90% confluency in 12-well plates, incubated in DMEM 0.2% FBS, and conditioned media was collected 72 h later. Media was cleared of cells by centrifuging at 2,000 r.p.m. for 5 min. Pro-MMP1, pro-MMP2 and VEGF-165 concentrations were analysed in conditioned media using ELISA kits (R&D Systems).

Animal studies. All animal work was done in accordance with a protocol approved by the MSKCC Institutional Animal Care and Use Committee. BALB/c nude and NOD/SCID female mice (NCI) age-matched between 5–7 weeks were used for xenografting studies. For primary tumour analysis, 1×10^6 viable single cells were re-suspended in a 1:1 mixture of PBS and growth-factor-reduced Matrigel (BD Biosciences) and injected orthotopically into mammary gland four in a total volume of 50 μl as previously described[12]. Primary tumour growth rates were analysed by measuring tumour length (L) and width (W), and calculating tumour volume based on the formula $\pi LW^2/6$. For experimental metastasis assays, 2×10^5 cells were re-suspended in 0.1 ml PBS and injected into the lateral tail vein. Lung metastatic progression was monitored and quantified using non-invasive bioluminescence as previously described[12].

Pharmacological inhibitors. Cetuximab (ImClone) was obtained from the MSKCC pharmacy. For inhibitor studies, 1 mg cetuximab was injected intraperitoneally bi-weekly. Injection with cetuximab at doses between 0.25 mg and 1 mg per injection achieve plasma drug concentrations within the corresponding range in cetuximab-treated cancer patients[35]. GM6001 (Ryss Lab) was injected intraperitoneally at a dose of 2 $mg\,kg^{-1}$ daily, which has previously been shown to be efficacious in preclinical mouse models[25]. Celecoxib (LKT laboratories) was mixed with a powdered rodent chow diet (Research diets) at a concentration of 1,000 parts per million (1 g celecoxib per 1 kg chow), and provided continuously during the course of the experiment. Previous pharmacokinetic studies demonstrate that celecoxib serum concentration in mice treated within this range are clinically attainable and sufficient to inhibit inflammation and prostaglandin synthesis in humans[22,26,36].

Trans-endothelial migration. HUVECs or primary HPMECs were seeded into collagen-coated trans-well inserts (1 μm pore size, BD Falcon) at 100,000 cells per well, and allowed to grow to confluence for 4 days. Tumour cells were pulsed with 5 μM cell tracker green (Invitrogen) for 30 min before being conditioned overnight in 0.2% FBS ECM media without growth factors. The next day, 50,000 tumour cells were seeded into trans-well inserts with or without a confluent endothelial monolayer, and the wells were fixed in 4% paraformaldehyde after 10 h. Cells on the apical side of each insert were scraped off and the trans-well membrane mounted onto slides. Migration to the basolateral side of the membrane was visualized with a Zeiss Axioplan2 immunofluorescent microscope at ×10 magnification. Pictures of 6–10 random fields across three replicate wells were captured for quantification using ImageJ software (NIH). In general, 150–200 counts per field of LM2 cells were seen to migrate in the absence of a monolayer, whereas 50 counts per field were seen to migrate through an endothelial barrier. Migration of the indicated lines was plotted as a percentage of migrating LM2 control cells.

Intravasation. Drug-treated mice were perfused with 5 ml PBS through the left ventricle. Three millilitres of blood perfusate was collected from the atrium and lysed two times using ACK lysis buffer (Cambrex). Total RNA was extracted from the remaining cells and used for qRT–PCR as described above. The presence of human circulating tumour cells was determined by the relative expression of human *GAPDH* normalized to murine β2-microglobulin.

Tumour and lung immunostaining. Mice were killed and perfused with PBS and 4% paraformaldehyde through the left ventricle, before tumours were extracted, fixed and paraffin-embedded. Immunohistochemical staining for CD31 (Santa Cruz), phospho-histone H3 (Upstate) and cleaved caspase-3 (Cell Signaling) was performed on paraffin-embedded tumour sections by the MSKCC Molecular Cytology Core Facility. Brightfield microscopic images were collected using an Axioplan2 microscopy system (Zeiss). Tumour cell proliferation (pH3) and apoptosis (cleaved caspase-3) were quantified using a combination of Adobe Photoshop (Adobe) and ImageJ software (NIH). In brief, the colour-picker function was used to identify manually the most darkly stained region of interest, with a constant fuzziness factor. The selected regions were feathered and expanded in a uniform manner, and thresholded into binary images, which were subsequently analysed in ImageJ. Morphometric analysis of CD31-stained vessels was achieved with Photoshop and Image Processing Tool Kit (Reindeer Graphics Inc.) based on a previously described protocol[37]. Angiogenic properties were then scored as a function of vessel density, average vessel length, average number of branch points per vessel, and lumen formation. On average, immunohistochemistry quantification was performed by taking pictures from five random fields per tumour, imaging at least three tumours per sample set. For immunofluorescence, tumours were fixed and frozen in OCT. Pericyte coverage of vessels was identified by double staining for the pericyte marker NG2 (Chemicon) and CD31 endothelial cell marker (BD Biosciences Pharmingen), followed by detection with fluorescently conjugated secondary antibodies (Jackson Immunoresearch). Permeability of tumour blood vessels was assessed by intravenous injection of rhodamine-conjugated dextran (70 kDa, Invitrogen) at 2 mg per 20 g body weight. After 1 h, mice were killed, tumours extracted, and 30-μm sections examined by fluorescence microscopy for vascular leakage. Immunofluorescent staining for pimonidazole adducts in

primary tumours was performed according to the Hypoxyprobe-1 staining kit (Chemicon).

To observe metastatic extravasation within the first 48 h of circulatory entry, tumour cells were labelled with 5 μM of cell tracker green (Invitrogen) for 1 h and inoculated into mice. Before sacrifice, mice were injected intravenously with rhodamine-conjugated lectin (Vector Laboratories) to stain the lung vasculature. Lungs were perfused with PBS, inflated through intra-tracheal injection, and extracted *en bloc*. Whole lungs were then scanned by two-photon confocal microscopy at ×63 using a Leica TCS SP2 microscope (DM IRE2 inverted stand). Representative three-dimensional images of stained capillaries and tumour cells were processed using Volocity v.3.6 (Improvision). To examine extravasating cells in the drug-treated mice, an alternative protocol was used. In this case, tumour cells did not retain cell tracker label during the extended time frame of the experiment and were alternatively co-stained with a monoclonal antibody that selectively detects human vimentin (Novocastra); anti-CD31 antibody (BD Biosciencies Pharmingen) was used to visualize lung capillaries. After fluorescent secondary antibody incubation, images were captured with a Leica TCS SP2 microscope (DMRXA2 upright stand) and processed using Volocity (Improvision). Quantification of lung metastasis was performed by creating montage images of whole-lung sections at ×10 magnification using an Axiovert 200M imaging system equipped with a motorized inverted stand (Zeiss). Image quantification was performed as described above using a combination of Adobe Photoshop (Adobe) and ImageJ software (NIH).

37. Wild, R., Ramakrishnan, S., Sedgewick, J. & Griffioen, A. W. Quantitative assessment of angiogenesis and tumor vessel architecture by computer-assisted digital image analysis: effects of VEGF-toxin conjugate on tumor microvessel density. *Microvasc. Res.* **59**, 368–376 (2000).